Nanoscale Research Letters

NANO EXPRESS Open Access

Efficiency Enhancement of Solid-State $CuInS_2$ Quantum Dot-Sensitized Solar Cells by Improving the Charge Recombination

Bowen Fu[1], Chong Deng[1,2] and Lin Yang[1*]

Abstract

Copper indium sulfide quantum dots ($CuInS_2$ QDs) were incorporated into a nanocrystalline TiO_2 film by using spin coating-assisted successive ionic layer adsorption and reaction process to fabricate $CuInS_2$ QD-sensitized TiO_2 photoelectrodes for the solid-state quantum dot-sensitized solar cell (QDSSC) applications. The result shows that the photovoltaic performance of solar cell is extremely dependent on the number of cycles, which has an appreciable impact on the coverage ratio of $CuInS_2$ on the surface of TiO_2 and the density of surface defect states. In the following high-temperature annealing process, it is found that annealing TiO_2/$CuInS_2$ photoelectrode at a suitable temperature would be beneficial for decreasing the charge recombination and accelerating the charge transport. After annealing at 400 °C, a significantly enhanced photovoltaic properties of solid-state $CuInS_2$ QDSSCs are obtained, achieving the power conversion efficiency (PCE) of 3.13%, along with an open-circuit voltage (V_{OC}) of 0.68 V, a short-circuit photocurrent density (J_{SC}) of 11.33 mA cm^{-2}, and a fill factor (FF) of 0.41. The enhancement in the performance of solar cells is mainly ascribed to the suppression of charge recombination and the promotion of the electron transfer after annealing.

Keywords: $CuInS_2$ quantum dots, Solar cells, Charge recombination, Electron transfer

Background

Owing to the merits of multiexciton generation and tunable band gap, quantum dot-sensitized solar cells (QDSSCs) have been considered as one of the ideal candidates for the new generation solar cells [1–4]. For the improvement of power conversion efficiency, it is essential to select a semiconductor material with the proper band gap. $CuInS_2$ (CIS) is a direct band gap I-III-VI_2 semiconductor compound with a near-optimal bulk band gap (1.5 eV) and has many advantageous features including the higher absorption coefficient (10^5 cm^{-1}), non-toxicity, and excellent stability [5–7]. To date, it has been demonstrated as a promising photosensitizer which has been successfully used in the field of QDSSCs [8–12].

The deposition process of QDs has a significant impact on the photovoltaic properties. As we have known, there are two major QD deposition approaches, i.e., the direct growth and post-synthesis assembly. Most of the researches are focused on the post-synthesis assembly method to fabricate solar cells [13–15]. For example, Wang et al. [16] controlled the Cu/In non-stoichiometric ratios of CIS QDs, achieving a PCE of 8.54%, which was a high efficiency for the CIS-based solar cells. Zhong's group [17] explored an alloyed Zn-Cu-In-Se (ZCISe) QD sensitizer and deposited ZCISe and CdSe QDs on mesoporous TiO_2, which achieved a PCE of 12.75%. However, this method suffers from the small loading amount of QDs and the disadvantageous status of electronic coupling between QD and TiO_2. To increase the QD loading and enhance the ability of efficient electron transfer to TiO_2, QDs could be directly grown on mesoporous TiO_2 film by successive ionic layer adsorption and reaction (SILAR) [18–20]. Furthermore, developing a strategy to accelerate the charge transport and enhance the device stability could greatly enhance the photovoltaic performance and versatility of QD-sensitized TiO_2 electrodes. It has been realized that the solid-state cell device architecture is desirable to retard the deterioration of long-term stability associated with liquid electrolytes [21,

* Correspondence: yanglin@hbu.edu.cn
[1]College of Physics Science and Technology, Hebei University, Baoding 071002, China
Full list of author information is available at the end of the article

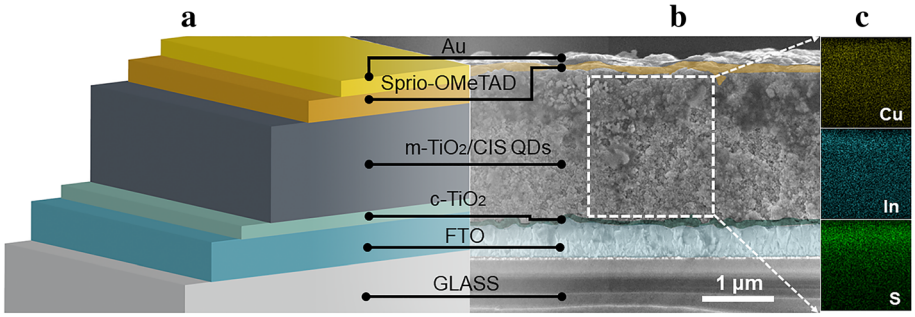

Fig. 1 **a** Schematic of the device architecture. **b** The cross-sectional SEM image of the solar cell (corresponding to the sample prepared with 20 cycles and annealed at 400 °C). **c** The elemental distribution maps of Cu, In, and S elements in TiO_2/CIS layer

22]. Despite the promise of solid-state cells, the efficiencies reported to date were lower. In the earlier reports, So and co-workers [23] fabricated a non-annealed heterojunction solar cell with a PCE of 1.16% by incorporating colloidal CIS nanocrystals into porous TiO_2 network. Zhou et al. [24] introduced In_2S_3 buffer layer into the solar cell based on $CuInS_2$, achieving a PCE of 1.06%. Chang et al. [25] developed the Cu_2S-$CuInS_2$-ZnS solid-state QDSSCs with a PCE of 2.52% through the SILAR process. The performance of such devices commonly gets worse due to the recombination between TiO_2 and hole conductor, which is faster than the analogous process in the devices with liquid electrolyte. A significant approach used to decrease recombination and increase efficiency is to modify the QDs absorber or TiO_2 photoanode, e.g., through increasing the loading amount of QDs, doping QDs to optimize the interfacial band alignment, or using of passivation layer.

In a previous study, we succeeded in fabricating solid-state devices using $CuInS_2$ quantum dot-sensitized TiO_2 photoanodes through SILAR method [26]. Herein, to further improve the efficiency of the device, we fabricated the solid-state solar cell by introducing CIS QDs into TiO_2 mesoporous layer through spin coating-assisted SILAR process, completely filling QDs in the pores of TiO_2 mesoporous layer. Through optimization of QD-sensitized TiO_2 films by using the precise deposition based on SILAR, together with the annealing treatment for the photoelectrodes, the solar cell consequently exhibits a PCE of 3.13%. As far as we know, this result is one of the best performances of CIS-based solid-state QDSSCs.

Methods

Materials

Indium acetate ($In(OAc)_3$, 99.99%) was purchased from Alfa Aesar. Copper(II) chloride dihydrate ($CuCl_2{\cdot}2H_2O$, 99.99%), sodium sulfide nonahydrate ($Na_2S{\cdot}9H_2O$, 99.9%), titanium isopropoxide (99.9%), hydrochloric acid (HCl, 37% in water), 2,2',7,7'-tetrakis-(*N*,*N*-di-p--methoxyphenylamine)-9,9'-spirobifluorene (spiro-OMeTAD, 99.5%), chlorobenzene (anhydrous, 99.8%), 4-tert-Butylpyridine (tBP), bis(trifluoromethane)sulfonimide lithium salt (Li-TFSI), and acetonitrile (anhydrous, 99.8%) were purchased from Sigma-Aldrich. TiO_2 paste (DSL 18NR-T) was obtained from Dyesol. All of the chemicals were utilized directly without further purification. Ultrapure deionized water was used for the preparation of aqueous solutions.

Preparation

A TiO_2 compact layer with a thickness of 70 nm was fabricated by spin-coating on the cleaned FTO glass at 4000 rpm for 30 seconds, using titanium isopropoxide (350 μL)

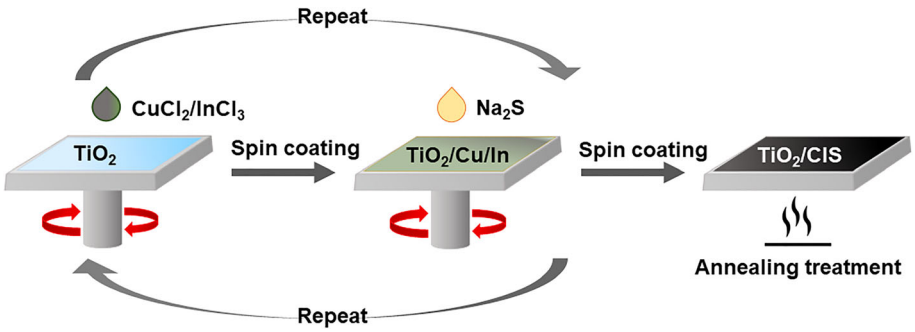

Fig. 2 Schematic of the process for fabricating CIS QD-sensitized TiO_2 photoelectrodes

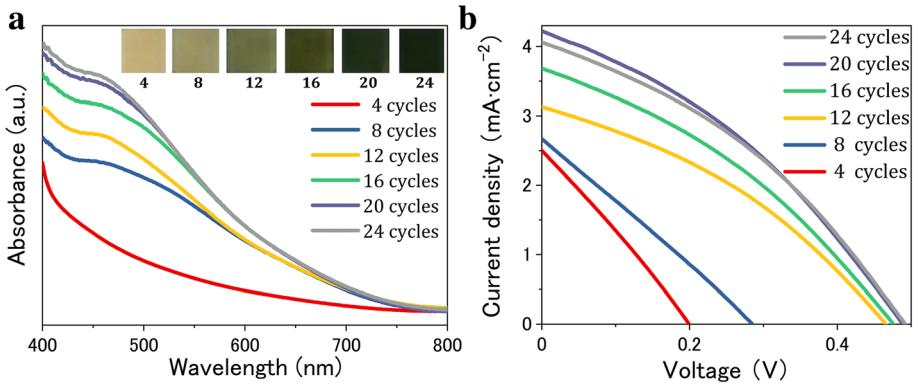

Fig. 3 **a** UV-vis absorption spectra of CIS QD-sensitized TiO_2 film prepared by spin coating-assisted SILAR with different cycles. The inset is the photographs of the corresponding photoelectrode films. **b** J-V curves of QDSSCs prepared at different cycles

and HCl (35 μL) diluted in ethanol (5 mL) as the precursor solution. The film was then annealed in the air starting at room temperature with 100 °C increments, holding for 10 min at each increment. At 500 °C, the film was annealed for an hour and then allowed to cool naturally. Next, the TiO_2 mesoporous layer was fabricated by spin-coating the diluted 18NR-T paste on the compact layer at 800 rpm for 10 s, followed by a heat treatment to achieve a 2-μm thickness layer.

CIS QD-sensitized TiO_2 thin film was prepared by spin coating-assisted SILAR. 80 μL of a mixture of 25 mM $CuCl_2$ and 50 mM $In(OAc)_3$ was dropped on the TiO_2 mesoporous layer and then spin-coated at 800 rpm for 20 s. Subsequently, 80 μL of 100 mM Na_2S was dropped and followed by spin-coating at 800 rpm for 20 s. The two steps were denoted as one cycle. Between each step, the film should be rinsed with deionized water and dried by N_2. In order to enhance the crystallinity of CIS QDs, the photoelectrodes were annealed under nitrogen atmosphere at 200–500 °C for 30 min. Subsequently, the hole transport material (HTM) was spin-coated under N_2 atmosphere by using a solution with a proper concentration of 300 mg of spiro-OMeTAD, 2.91 μL of chlorobenzene, 28.77 μL of tBP, and 126 μL of Li-TFSI. Finally, gold was deposited by thermal evaporation as a counter electrode and the active area of 0.09 cm^2 was defined.

Table 1 Photovoltaic parameters obtained from the J-V curves of QDSSCs using TiO_2/CIS films prepared with different cycles as photoelectrodes

Cycles	V_{OC} (V)	J_{SC} (mA cm^{-2})	FF	PCE (%)
4	0.20	2.49	0.28	0.14
8	0.28	2.65	0.26	0.20
12	0.46	3.12	0.36	0.51
16	0.47	3.68	0.36	0.62
20	0.48	4.21	0.37	0.75
24	0.49	4.05	0.36	0.72

Characterization

UV-vis absorption spectra were recorded on a UV-vis spectrophotometer (Perkin Elmer Lambda 950). Cross-sectional scanning electron microscopy (SEM) was characterized by FEI nova nano SEM450. The elemental mappings were characterized by an ORBIS energy dispersive spectroscopy (EDS), an accessory of the SEM. The current density-voltage (J-V) measurements for solar cells were carried out under the illumination of a solar simulator equipped with a 300 W xenon lamp (Model No. XES-100S1, SAN-EI, Japan) under the standard test conditions (25 °C, AM1.5, 100 mW·cm^{-2}). The incident photon-to-current conversion efficiency (IPCE) was measured by an Enlitech QER3011 system equipped with a 150 W xenon light source. Electrochemical impedance spectroscopy (EIS) was carried out on an electrochemical workstation (Zahner, Zennium) under dark conditions at different forward biases from − 0.1 to − 0.5 V, applying a 20-mV AC sinusoidal signal over the constantly applied bias with the frequency ranging from 1 to 0.1 Hz. Time-resolved photoluminescence (TRPL) was employed by PL Spectrometer (Edinburgh Instruments, FLS 900), excited with a picosecond pulsed diode laser (EPL 445) at a wavelength of 543 nm.

Results and Discussion

A schematic of the device architecture is shown in Fig. 1, incorporating with the cross-sectional SEM image covered by false colors to distinguish the different layers prepared in the device. The uniform distribution of particles and superior contact between interfaces can improve the electrical conductivity of thin films that would enhance the charge carrier transfer [27–29]. The elemental mapping of CIS-sensitized TiO_2 mesoporous film electrode is also performed through energy dispersive X-ray (EDX) analysis, providing clear evidence to prove the uniform distribution of CIS throughout the film.

The procedure of fabricating CIS QD-sensitized TiO_2 photoelectrodes in our work is schematically illustrated

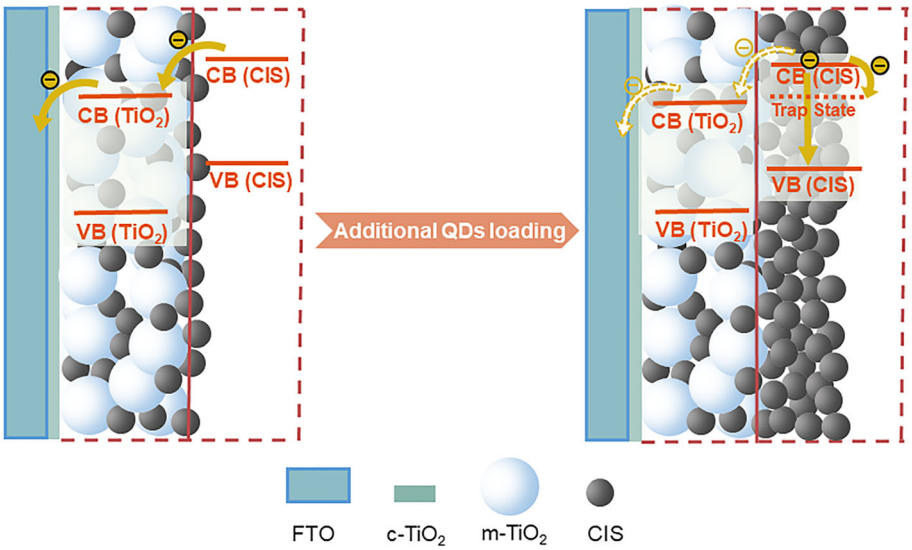

Fig. 4 Schematic diagram of the major pathways of electron transfer and charge recombination existing in QDSSCs

in Fig. 2. It is worth pointing out that the spin coating-assisted SILAR method adopted in this work can control the amount of QD depositions accurately. The amount of CIS QDs incorporated in the mesoporous TiO_2 layer was evaluated using the UV-vis absorption spectra. Figure 3a shows the variation of spectra with different spin coating-assisted SILAR cycles. After four cycles performed, only a much smaller amount of CIS QDs is deposited in TiO_2 film, as indicated by the lower absorbance of TiO_2/CIS photoelectrode. An increase in the number of cycles results in an increase of absorbance and a slight red shift of the absorption onset, corresponding to the color change of photoelectrodes from dark yellow to black, as shown in the inset of Fig. 3a. Subsequently, we fabricated and characterized the photovoltaic devices with TiO_2/CIS photoelectrodes.

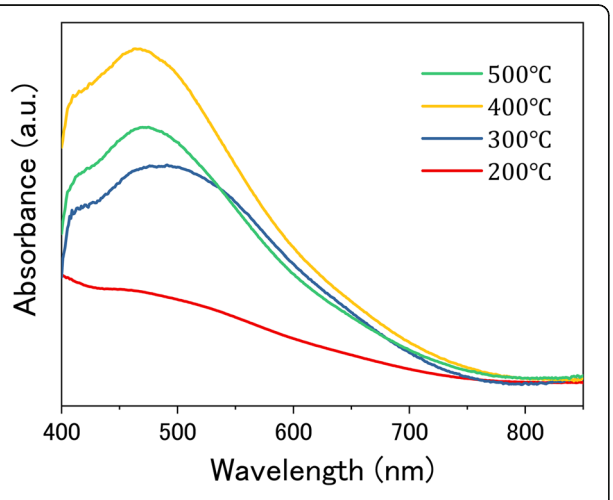

Fig. 5 UV-vis absorption spectra of TiO_2/CIS photoelectrodes with annealing treatment at different temperatures

Figure 3b shows the J-V curves of CIS QDSSCs. With increasing the number of spin coating-assisted SILAR cycles, both J_{SC} and PCE gradually increase from 2.49 mA cm^{-2} and 0.14% for 4 cycles to 4.21 mA cm^{-2} and 0.75% for 20 cycles, and then decrease to 4.05 mA cm^{-2} and 0.72% for 24 cycles, respectively, as clearly revealed in Table 1. This result demonstrates that the cycle process in the initial stage aims to increase the coverage of CIS QDs through refilling the uncovered areas in TiO_2 mesoporous layer. It is no doubt that an enhancement of QD loading amount and a formation of QDs monolayer on the surface of TiO_2 photoanode are advantageous to generate much more excited electrons under light illumination, which would increase the photocurrent of solar cells [30]. Moreover, a higher surface coverage for TiO_2 is achieved with the increase of CIS QDs loading amount. The decrease of surface areas exposed directly to the HTM is favorable for the suppression of charge recombination process occurring at TiO_2/HTM interface, thus leading to a dramatic increase of V_{OC} and an improvement of FF, especially in the early cycles. However, the thickness of the CIS layer could continuously increase after each spin coating-assisted SILAR cycle owing to the additional QD loadings. Because of the increased generation probability of charge recombination in CIS layer, the process of transporting photogenerated electrons from the QD layers to the TiO_2 matrix will become more difficult, as shown in the schematic drawing of Fig. 4. The electrons in the QD conduction band (CB) can be trapped by the surface defect states [31, 32], which serve as the recombination

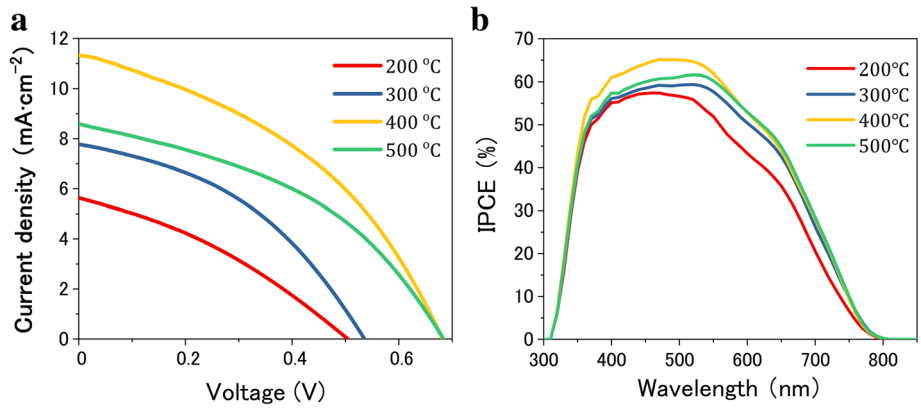

Fig. 6 a J-V curves and **b** IPCE spectra of the cell devices based on TiO_2/CIS photoelectrodes with annealing treatment at different temperatures

centers, eventually giving a deterioration of the device. Meanwhile, the undesirable recombination path of the electrons in QD CB and the holes in QD VB could hinder the electron injection from CIS into TiO_2 as well. Therefore, after the evaluation and verification of these effects, it clearly indicates that the ideal number of cycles (20) should be performed for the deposition CIS QDs in this work.

Afterward, the influence of annealing treatment on the performance of photovoltaic devices is evaluated. Figure 5 presents the evolution of the absorption of CIS QD-sensitized TiO_2 films with different annealing temperatures. It is found that the absorption is improved gradually with increasing the annealing temperature. The absorbance gets to a saturation value at the temperature of 400 °C. Simultaneously, excessive annealing treatment would deteriorate CIS QD sensitizer due to the occurrence of aggregation and oxidization [33]. It results in a decrease in absorbance when the annealing temperature is further elevated to 500 °C. Therefore, it is inferred that an excessive increase of annealing temperature (> 400 °C) is disadvantageous to the performance of cell devices.

The J-V curves of QDSSCs which were measured under simulated AM1.5 sunlight illumination are shown in Fig. 6a, comparing the photocurrent-photovoltage characteristics of cell devices with different annealing temperatures. The detailed parameters are listed in Table 2. The device based on the photoelectrode annealed at 200 °C shows a much lower J_{SC} of 5.63 mA cm^{-2}. A relatively higher J_{SC} of 7.76 mA cm^{-2} was obtained by annealing the TiO_2/CIS photoelectrode at 300 °C. At 400 °C, the device exhibits the highest PCE of 3.13%, along with V_{OC} of 0.68 V, J_{SC} of 11.33 mA cm^{-2}, and FF of 0.41. The enhanced J_{SC} results from the beneficial light-harvesting enhancement over the UV-vis spectrum for the photoelectrodes with annealing treatment at a higher temperature. Nevertheless, with increasing the temperature up to 500 °C, it is no longer able to bring an improvement in the performance of solar cells, unfortunately causing a significant decline in J_{SC} and PCE. So the film annealed at 400 °C exhibits the best photovoltaic performance as compared with the other three samples. To assess the light absorption and the electron generation characteristics, IPCE spectra are shown in Fig. 6b. It exhibits a strong photoresponse with a value of 66% in the visible wavelength range between 400 and 550 nm for QDSSCs with the annealing temperature of 400 °C, with nearly 20% enhancement compared to that of 200 °C. The higher IPCE response generally ascribed the outstanding absorptivity of QDs in the spectral region. According to the spectral, it can be found that a wider response wavelength range and a higher IPCE value appeared, which is in accordance with the variation tendency of J_{SC} as observed in J-V measurement. The result could be supported by the interpretation that the proper annealing treatment is potentially more favorable for the formation of an enforced interface connection between CIS and TiO_2, thus leading to the effective electron transfer in QDSSCs [34].

To analyze the transfer and recombination process of charge carrier, the devices are further investigated by EIS. Figure 7a displays the Nyquist plot of the obtained EIS results at − 0.4 V bias, and the fitted values evaluated from the equivalent circuit are listed in Table 3, where the electron lifetime can be estimated by $\tau_n = R_r \times C_\mu$ [35–37]. At the HTM/counter electrode interface, the charge transfer resistance R_{ct} which is related to the

Table 2 Photovoltaic parameters obtained from the J-V curves of QDSSCs using TiO_2/CIS films annealed at different temperatures as photoelectrodes

Temperatures	V_{OC} (V)	J_{SC} (mA cm^{-2})	FF	PCE (%)
200 °C	0.50	5.63	0.37	1.04
300 °C	0.53	7.76	0.41	1.68
400 °C	0.68	11.33	0.41	3.13
500 °C	0.68	8.58	0.42	2.44

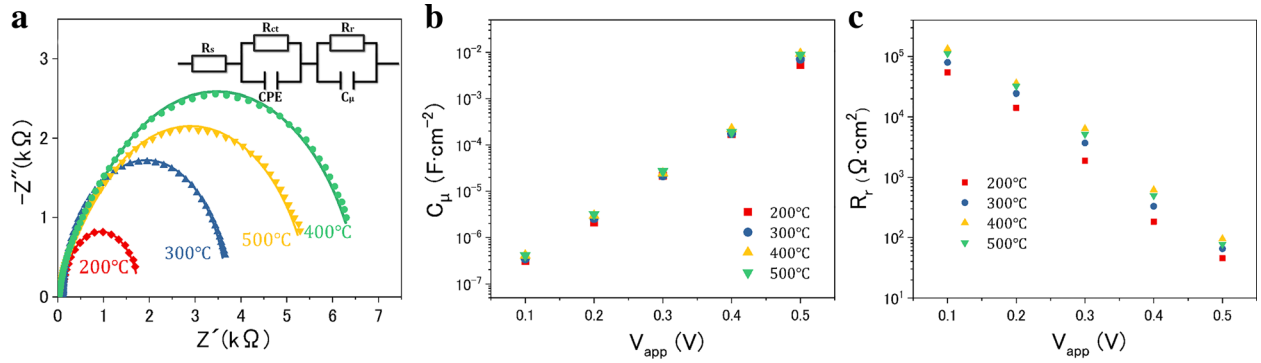

Fig. 7 **a** EIS spectra of the cell devices measured in the dark at − 0.4 V bias. The inset in **a** illustrates the equivalent circuit simulated to fit the impedance spectra. R_S represents the substrate resistance. R_{ct} and CPE represent the charge transfer resistance and capacitance at the HTM/counter electrode interface, respectively. R_r and C_μ represent the recombination resistance and chemical capacitance at the photoelectrode/HTM interface, respectively. **b** C_μ and **c** R_r at different applied voltages (V_{app}), calculated from the fitting of the impedance spectra

high-frequency semicircles presents no obvious differences, while the same HTM and counter electrode were employed in the present QDSSCs. The simulated datum of recombination resistance R_r which is related to the low-frequency semicircles represents the electron transfer process at photoelectrode/HTM interface. This datum for QDSSCs with TiO_2/CIS photoelectrode annealed at 400 °C is larger as compared with the others, which is attributed to the suppressed interfacial recombination, resulting in an enhanced V_{OC}. Furthermore, the long-lived charge carriers could favor the improvement of charge collection efficiency, thereby contributing to the significant progress in IPCE and J_{SC} [6]. According to Table 3, in the present case, the TiO_2/CIS photoelectrode annealed at 400 °C is indicated to remain the highest value of τ_n, ~ 117 ms, thus yielding the highest value of J_{SC} as observed in the J-V measurement. Nevertheless, τ_n falls to ~ 78 ms when the higher temperature of 500 °C was applied. The V_{app}-dependent C_μ and R_r extracted from EIS measurements are illustrated in Fig. 7b and c, respectively. C_μ increases exponentially with the V_{app}, as expected from the theoretical basis. The similar C_μ values of all the cells illustrate that different annealing temperatures do not produce a shift on the position of TiO_2 CB [38, 39]. In addition, with increasing the temperature from 200 to 400 °C, the R_r value is improved gradually. Since the recombination rate occurring at photoelectrode/HTM interface is inversely proportional to R_r [39], the greater value of R_r means the reduced recombination rate occurring in the solar cell based on TiO_2/CIS photoelectrode annealed at 400 °C. Overall, from these EIS results, it can be concluded that the cell devices show a large recombination rate rather than a shift of TiO_2 CB. It also supports the lower recombination rate and longer electron lifetime for the solar cell based on TiO_2/CIS photoelectrode annealed at 400 °C, which is conducive to the enhanced V_{OC}, J_{SC}, and FF values for cells undergoing annealing treatment on photoelectrodes as observed in the J-V curves.

In order to further clarify the effect of annealing temperature on charge transfer, the time-resolved transient photoluminescence (TRPL) spectra of the samples are displayed in Fig. 8. It can be seen that the PL lifetime of the photoanode significantly decreases with the increase of the annealing temperature, which indicates that more electrons could transfer from CIS to TiO_2 efficiently, reducing the probability of internal photogenerated carrier recombination inside QDs to some extent. According to the calculation of the rate of electron transfer (k_{et}) [40, 41], it can be observed that the solar cell based on TiO_2/CIS photoelectrode annealed at 400 °C has the higher k_{et} value of $1.17 \times 10^7\ s^{-1}$, thus providing excellent charge transfer performance of QDSSCs. Consequently, it provides further evidence to support that the proper annealing treatment is potentially more favorable for obtaining an effective connection at TiO_2/QDs interfaces [33], which is extremely beneficial for the transport of charge carrier in QDSSCs, thereby leading to a higher efficiency.

Table 3 Fitted values of resistance, capacitance, and electron lifetime in EIS spectra at − 0.4 V bias

Temperatures	R_s (Ω)	R_{ct} (Ω cm^2)	CPE (mF/cm^2)	R_r (Ω·cm^2)	C_μ (mF/cm^2)	τ_n (ms)
200 °C	67.87	11.88	0.40	153	0.12	18
300 °C	65.58	17.17	0.50	329	0.14	46
400 °C	60.68	16.66	0.40	618	0.19	117
500 °C	64.36	15.68	0.44	495	0.16	79

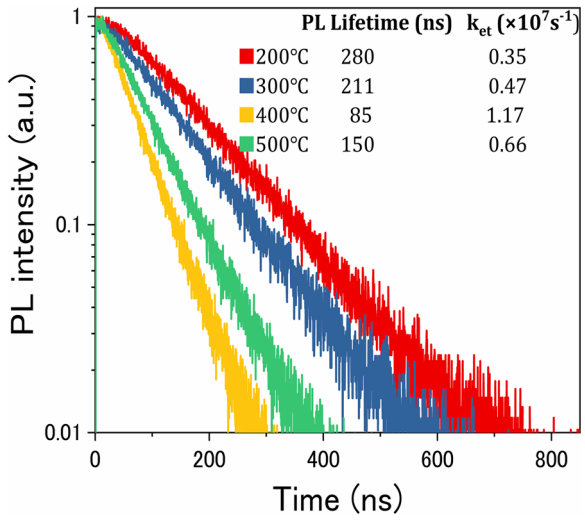

Fig. 8 TRPL spectra of CIS QD-sensitized TiO_2 films. The inset presents the PL lifetime and the rate of electron transfer

Conclusions

In summary, CIS QD-sensitized TiO_2 films were obtained by the spin coating-assisted SILAR method and further used as the promising photoelectrodes for solid-state QDSSCs. The spin coating-assisted SILAR method can control the amount of QD deposition accurately. Increasing the number of cycles could enhance the absorption ability, leading to more electrons generated under light illumination. The charge recombination process occurring at TiO_2/HTM interface would be suppressed with the increase in the QD loading amount as well. However, there would appear the undesirable recombination pathways in the thicker CIS layer due to the excessive increase in the number of cycles, which is extremely detrimental to the device performance. The following high-temperature annealing treatment plays a critical role in enhancing the contact between CIS QDs and TiO_2 photoanode and reducing the probability of internal photogenerated carrier recombination. According to J-V characteristics and EIS results, the most suitable annealing temperature for TiO_2/CIS photoelectrode film should be 400 °C, which shows the highest efficiency of 3.13% and the longest electron lifetime of 117 ms. IPCE of 66% between 400 and 550 nm and k_{et} of $1.17 \times 10^7\ s^{-1}$ are also achieved with the solid-state QDSSCs. This work may enlighten the way to fabricate the other kinds of sensitized photoelectrodes with high photovoltaic performance, and the next work will focus on improving the stability of cell devices.

Abbreviations

CB: Conduction band; CIS QDs: Copper indium sulfide quantum dots; EDS: Energy dispersive spectroscopy; EIS: Electrochemical impedance spectroscopy; FF: Fill factor; IPCE: Incident photon-to-current conversion efficiency; J_{SC}: Short-circuit photocurrent density; PCE: Power conversion efficiency; QDSSCs: Quantum dot-sensitized solar cells; SEM: Scanning electron microscopy; SILAR: Successive ionic layer adsorption and reaction; TRPL: Time-resolved photoluminescence; VB: Valence band; V_{OC}: Open-circuit voltage

Acknowledgements

The authors greatly acknowledge the Hebei Key Laboratory of Opticelectric Information and Materials and the National & Local Joint Engineering Laboratory of New Energy Photoelectric Devices for the measurement assistance.

Funding

This research was supported by the National Natural Science Foundation of China (No. 11604072), Scientific and Technological Research Project of Hebei Province (No. QN2015008), and the Preferentially Supported Project for People Studying Abroad of Hebei Province (No. C2015005010). The authors also wish to thank the Hebei Key Laboratory of Opticelectric Information and Materials and the National & Local Joint Engineering Laboratory of New Energy Photoelectric Devices for the measurement assistance.

Availability of Data and Materials

All the data are fully available without restrictions.

Authors' Contributions

YL supervised the whole project and interpreted the results. FB performed the experiments and data analysis. DC classified and analyzed the reference papers. All authors contributed to the general discussion. All authors read and approved the final manuscript.

Competing Interests

The authors declare that they have no competing interests.

Publisher's Note

Author details

[1]College of Physics Science and Technology, Hebei University, Baoding 071002, China. [2]Key Laboratory of Semiconductor Photovoltaic Technology of Inner Mongolia Autonomous Region, School of Physical Science and Technology, Inner Mongolia University, Hohhot 010021, China.

Received: 21 February 2019 Accepted: 30 April 2019
Published online: 06 June 2019

References

1. Kamat PV, Tvrdy K, Baker DR, Radich JG (2010) Beyond photovoltaics: semiconductor nanoarchitectures for liquid-junction solar cells. Chem Rev 110:6664–6688
2. Green MA, Bremner SP (2017) Energy conversion approaches and materials for high-efficiency photovoltaics. Nat Mater 16:23–34
3. Nozik AJ, Beard MC, Luther JM, Law M, Ellingson RJ, Johnson JC (2010) Semiconductor quantum dots and quantum dot arrays and applications of multiple exciton generation to third-generation photovoltaic solar cells. Chem Rev 110:6873–6890
4. Zhou R, Yang Z, Xu J, Cao G (2018) Synergistic combination of semiconductor quantum dots and organic-inorganic halide perovskites for hybrid solar cells. Coord Chem Rev 374:279–313
5. Peng Z, Liu Y, Zhao Y, Chen K, Cheng Y, Kovalev VL, Chen W (2014) ZnSe passivation layer for the efficiency enhancement of $CuInS_2$ quantum dots sensitized solar cells. J Alloys Compd 587:613–617
6. Pan Z, Morasero I, Shen Q, Zhang H, Li Y, Zhao K, Wang J, Zhong X (2014) Bisquert J. High-efficiency "Green" quantum dot solar cells. J Am Chem Soc 136:9203–9210
7. Arici E, Sariciftci NS, Meissner D (2003) Hybrid solar cells based on nanoparticles of $CuInS_2$ in organic matrices. Adv Funct Mater 13:165–171
8. Ilaiyaraja P, Rakesh B, Das TK, Mocherla PSV, Sudakar C (2018) $CuInS_2$ quantum dot sensitized solar cells with high $V_{OC} \approx 0.9$ V achieved using microsphere-nanoparticulate TiO_2 composite photoanode. Sol Energy Mater Sol Cells 178:208–222

9. Meng W, Zhou X, Qiu Z, Liu C, Chen JL, Yue W, Wang M, Bi H (2016) Reduced graphene oxide-supported aggregates of $CuInS_2$ quantum dots as an effective hybrid electron acceptor for polymer-based solar cells. Carbon 96:532–540
10. Deng C, Fu B, Wang Y, Yang L (2018) Fabrication of water-soluble $CuInS_2$ quantum dots by hot-injection eethod and phase transfer strategy. Nano 13:1850114
11. Higashimoto S, Murano M, Arase T, Mukai S, Azuma M (2017) Takahashi M. Highly qualified copper-indium sulfide colloids prepared in water under microwave irradiation and their applications to the TiO_2 based quantum dot-sensitized solar cells. Sol Energy Mater Sol Cells 169:203–209
12. Xing H, Zhang Q, Huang X, Li D, Luo Y, Meng Q (2011) Aqueous colloidal $CuInS_2$ for quantum dot sensitized solar cells. J Mater Chem 21:15903–15905
13. Sixto G, Iván MS, Lorena M, Nestor G, Teresa LV, Roberto G, Diguna LJ, Qing S, Taro T, Juan B (2009) Improving the performance of colloidal quantum-dot-sensitized solar cells. Nanotechnology 20:295204
14. Malak ST, Lafalce E, Jung J, Lin CH, Smith MJ, Yoon YJ, Lin Z, Vardeny ZV, Tsukruk VV. Enhancement of optical gain characteristics of quantum dot films by optimization of organic ligands. J Mater Chem C. 2016;4:10069–81.
15. Pan Z, Rao H, Mora-Seró I, Bisquert J, Zhong X (2018) Quantum dot-sensitized solar cells. Chem Soc Rev 47:7659–7702
16. Wang G, Wei H, Shi J, Xu Y, Wu H, Luo Y, Li D, Meng Q (2017) Significantly enhanced energy conversion efficiency of $CuInS_2$ quantum dot sensitized solar cells by controlling surface defects. Nano Energy 35:17–25
17. Wang W, Feng W, Du J, Xue W, Zhang L, Zhao L, Li Y, Zhong X (2018) Cosensitized quantum dot solar cells with conversion efficiency over 12%. Adv Mater 30:1705746
18. Li TL, Lee Y, Teng H (2012) High-performance quantum dot-sensitized solar cells based on sensitization with $CuInS_2$ quantum dots/CdS heterostructure. Energy Environ Sci 5:5315–5324
19. Zhang X, Liu J, Johansson EMJ (2015) Efficient charge-carrier extraction from Ag_2S quantum dots prepared by the SILAR method for utilization of multiple exciton generation. Nanoscale 7:1454–1462
20. Sun L (2016) Employing ZnS as a capping material for PbS quantum dots and bulk heterojunction solar cells. Sci China Mater 59:817–824
21. Feng W, Li Y, Du J, Wang W, Zhong X (2016) Highly efficient and stable quasi-solid-state quantum dot-sensitized solar cells based on a superabsorbent polyelectrolyte. J Mater Chem A 4:1461–1468
22. Park JP, Heo JH, Im SH, Kim S-W (2016) Highly efficient solid-state mesoscopic PbS with embedded CuS quantum dot-sensitized solar cells. J Mater Chem A 4:785–790
23. So D, Pradhan S, Konstantatos G (2016) Solid-state colloidal $CuInS_2$ quantum dot solar cells enabled by bulk heterojunctions. Nanoscale 8:16776–16785
24. Zhou Z, Yuan S, Fan J, Hou Z, Zhou W, Du Z, Wu S (2012) $CuInS_2$ quantum dot-sensitized TiO_2 nanorod array photoelectrodes: synthesis and performance optimization. Nanoscale Res Lett 7:652–652
25. Chang JY, Su LF, Li CH, Chang CC, Lin JM (2012) Efficient "green" quantum dot-sensitized solar cells based on Cu_2S-$CuInS_2$-ZnSe architecture. Chem Commun (Camb) 48:4848–4850
26. Yang L, Ma Y, Liu J, Mai Y (2016) Improving the performance of solid-state quantum dot-sensitized solar cells based on TiO_2/$CuInS_2$ photoelectrodes with annealing treatment. RSC Adv 6:92869–92873
27. Gratzel M (2005) Solar energy conversion by dye-sensitized photovoltaic cells. Inorg Chem 44:6841–6851
28. Zhao H, Huang F, Hou J, Liu Z, Wu Q, Cao H, Jing Q, Peng S, Cao G (2016) Efficiency enhancement of quantum dot sensitized TiO_2/ZnO nanorod arrays solar cells by plasmonic Ag nanoparticles. ACS Appl Mater Inter 8: 26675–26682
29. Evangelista RM, Makuta S, Yonezu S, Andrews J, Tachibana Y (2016) Semiconductor quantum dot sensitized solar cells based on ferricyanide/ferrocyanide redox electrolyte reaching an open circuit photovoltage of 0.8 V. ACS Appl Mater Inter 8:13957–13965
30. Li W, Zhong X (2015) Capping ligand-induced self-assembly for quantum dot sensitized solar cells. J Phys Chem Lett 6:796–806
31. Li L, Pandey A, Werder DJ, Khanal BP, Pietryga JM, Klimov VI (2011) Efficient synthesis of highly luminescent copper indium sulfide-based core/shell nanocrystals with surprisingly long-lived emission. J Am Chem Soc 133: 1176–1179
32. Zhao K, Pan Z, Zhong X (2016) Charge recombination control for high efficiency quantum dot sensitized solar cells. J Phys Chem Lett 7:406–417
33. Pan Z, Zhang H, Cheng K, Hou Y, Hua J, Zhong X (2012) Highly efficient inverted type-I CdS/CdSe core/shell structure QD-sensitized solar cells. ACS Nano 6:3982–3991
34. Fan S, Kim D, Kim J, Jung D, Kang S, Ko J (2009) Highly efficient CdSe quantum-dot-sensitized TiO_2 photoelectrodes for solar cell applications. Electrochem Commun 11:1337–1339
35. Yu X, Liao J, Qiu K, Kuang D, Su C (2011) Dynamic study of highly efficient CdS/CdSe quantum dot-sensitized solar cells fabricated by electrodeposition. ACS Nano 5:9494–9500
36. Yang L, Zhou R, Lan J, Zhang Q, Cao G, Zhu J (2014) Efficient band alignment for $Zn_xCd_{1-x}Se$ QD-sensitized TiO_2 solar cells. J Mater Chem A 2:3669
37. Yang L, Mccue C, Zhang Q, Uchaker E, Mai Y, Cao G (2015) Highly efficient quantum dot-sensitized TiO_2 solar cells based on multilayered semiconductors (ZnSe/CdS/CdSe). Nanoscale 7:3173–3180
38. Boix PP, Larramona G, Jacob A, Delatouche B, Mora-Sero I, Bisquert J (2012) Hole transport and recombination in all-solid Sb_2S_3-sensitized TiO_2 solar cells using CuSCN as hole transporter. J Phys Chem C 116:1579–1587
39. Zarazúa I, Esparza D, López-Luke T, Ceja-Fdez A, Reyes-Gomez J, Mora-Seró I, de la Rosa E (2016) Effect of the electrophoretic deposition of Au NPs in the performance CdS QDs sensitized solar cells. Electrochimica Acta 188:710–717
40. Kongkanand A, Tvrdy K, Takechi K, Kuno M, Kamat PV (2008) Quantum dot solar cells. Tuning photoresponse through size and shape control of CdSe-TiO_2 architecture. J Am Chem Soc 130:4007–4015
41. Robel I, Kuno M, Kamat PV (2007) Size-dependent electron injection from excited CdSe quantum dots into TiO_2 nanoparticles. J Am Chem Soc 129: 4136–4137